optica

Ultralow jitter silica microcomb

Dongin Jeong,[1,†] **Dohyeon Kwon,**[2,†] **Igju Jeon,**[2] **In Hwan Do,**[1] **Jungwon Kim,**[2,*] 🄳 **and Hansuek Lee**[1,3,4]

[1]*Graduate School of Nanoscience and Technology, Korea Advanced Institute of Science and Technology (KAIST), Daejeon 34141, South Korea*
[2]*School of Mechanical and Aerospace Engineering, Korea Advanced Institute of Science and Technology (KAIST), Daejeon 34141, South Korea*
[3]*Department of Physics, Korea Advanced Institute of Science and Technology (KAIST), Daejeon 34141, South Korea*
[4]*e-mail: hansuek@kaist.ac.kr*
Corresponding author: jungwon.kim@kaist.ac.kr

Silica microcombs have a high potential for generating tens of gigahertz of optical pulse trains with ultralow timing jitter, which is highly suitable for higher speed and higher bandwidth information systems. So far, the accurate characterization of timing jitter in microcombs has been limited by the measurement methods—although theoretically predicted to be >20 dB better performance, the true performance has not been accurately measured until now. Here, using a self-heterodyne-based measurement method with 20 zs/Hz$^{1/2}$ resolution, we show that 2.6-fs rms timing jitter is possible for 22-GHz silica microcombs. We identified their origins, which suggests that silica microcombs may achieve 200-as-level jitter by better intensity noise control. This jitter performance can greatly benefit many high-speed and high-bandwidth applications including analog-to-digital conversion, microwave generation, and optical communications. © 2020 Optical Society of America under the terms of the OSA Open Access Publishing Agreement

https://doi.org/10.1364/OPTICA.390944

Microresonator-based Kerr optical frequency combs (microcombs) [1,2] have evolved to be a very powerful light source for generating soliton optical pulse trains from compact and integrated platforms. There has recently been remarkable progress in implementation platforms [2–5] and applications [6–9]. Timing jitter, i.e., fast timing fluctuations of optical pulses from perfectly periodic temporal positions, is one of the most important performance measures of periodic signal generators such as microcombs. It also corresponds to the integrated phase noise in the repetition rate of optical frequency combs. Low-jitter optical frequency combs can be used for various applications including low-phase-noise microwave generation [10,11], synchronization of ultrafast X-ray science experiments [12,13], ranging and distance metrology [14,15], and clocks for high-performance data converters [16,17], telecommunications [18], and clock distribution networks [19]. Although mode-locked laser-based optical frequency combs can generate subfemtosecond-jitter optical pulse trains [20–22], their repetition rates have been so far limited to the subgigahertz range.

For higher-speed and higher-bandwidth telecommunications and signal processing applications, repetition-rates of >10 GHz are highly desirable. Since microcombs can provide such high repetition rates ranging from ~10 GHz up to ~1 THz, there have been research efforts for characterizing timing jitter (phase noise in repetition rate) of various microcombs, including silica [23–26], silicon nitride [27–29], and crystalline MgF$_2$ [30,31] microcombs.

Among different material platforms, silica microcombs [7,23–26] have many advantages for telecommunication and signal processing applications. Their typical repetition rates are in the tens of gigahertz range, which is highly suitable for analog-to-digital conversion [17], microwave generation [10,11], clock distribution networks [19], and 5G communications working in the 24–47 GHz range [32]. Further, silica microresonators can achieve an ultrahigh Q-factor, 8.75×10^8 [33], which can be fabricated as a fully integrated system using CMOS-compatible processes [34] with low pumping power proportional to $1/Q^2$ [35]. So far, the accurate characterization and optimization of timing jitter in microcombs have been limited by the measurement methods [23–26,28–31]. The best repetition-rate phase noise measured at 1-MHz offset frequency was limited to −152 dBc/Hz at 15-GHz carrier frequency (i.e., 1.6×10^{-37} s^2/Hz) [26], even though the theoretical predictions [28,36] have shown that it can achieve more than 20 dB better performance.
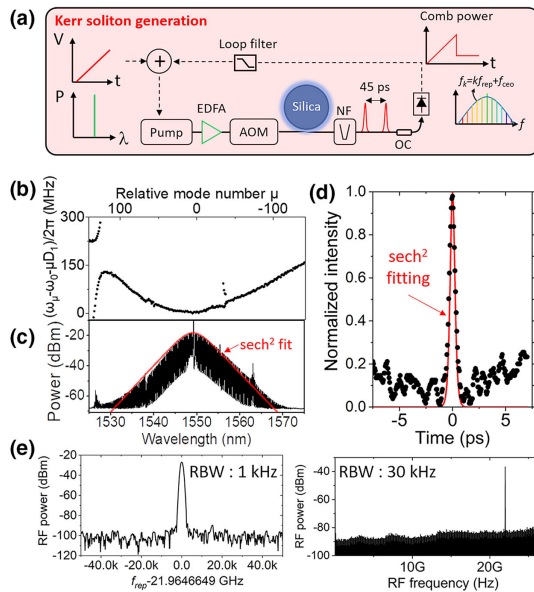
In this Letter, we characterize the low timing jitter of a 22-GHz soliton pulse train generated from a silica microcomb using a high-resolution fiber delay line-based self-heterodyne method [37,38]. The timing jitter power spectral density (PSD) at 1 MHz offset frequency is 7.3×10^{-40} s^2/Hz, with integrated rms timing jitter of 2.6 fs (integration bandwidth, 10 kHz–3 MHz). The measured timing jitter at 1-MHz offset frequency corresponds to ~23 dB lower than the previous state of the art [26], which was limited by the measurement resolution, and our result elucidates the true timing performance of the microcombs for the first time (see Fig. S1 of Supplement 1 for comparison with previous state-of-the-art performances of microcombs).

The soliton generation setup and measured characteristics are summarized in Fig. 1. A silica wedge resonator having a thickness of 8.2 μm, a diameter of 3 mm, and a wedge angle of 23° was fabricated through semiconductor processing [33]. The intrinsic Q-factor of the resonator was 106 million. Fine tuning of the wedge angle and diameter was performed to achieve anomalous

dispersion and minimization of mode crossing [25,39]. The measured dispersion is shown in Fig. 1(b), where the convex down profile indicates anomalous dispersion with 16.5 kHz at 1550 nm.

The soliton generation was achieved by the power-kicking method and active-capture technique [40,41] [Fig. 1(a)]. A fiber laser with narrow linewidth was used as a pump source. The acousto-optic modulator with fast rise time was used for fast power modulation within a few microseconds. The servo box feeds its output to the piezoelectric transducer (PZT) in the pump laser to lock and stabilize the soliton mode. The soliton pulse was generated with the pump power of 40 mW coupled to the silica resonator through a tapered fiber. The optical spectrum with the squared hyperbolic secant envelope is shown in Fig. 1(c), which also displays the spurs associated with the mode crossing. From the envelope, the transform-limited full width at half-maximum (FWHM) pulse width is ∼290 fs. The intensity autocorrelation result [Fig. 1(d)] shows ∼344 fs FWHM pulse width when fitted by sech^2 shape. The measured RF spectra in Fig. 1(e) show a single narrow peak at the fundamental repetition rate of 21.96 GHz with a high signal-to-noise ratio.

Timing jitter of the silica microcomb is characterized by a fiber delay-line-based self-heterodyne method [27,38] (Fig. 2). There are two main advantages to using this method. First, it is a reference-source-free method: it does not require another phase-locked, lower-noise reference oscillator with the same repetition rate for jitter characterization. Second, subfemtosecond-resolution timing jitter characterization of a free-running optical frequency comb is possible without any feedback signal to the comb under test. This is a useful property for characterizing microcombs since, unlike mode-locked lasers, many types of microcombs are

not equipped with separate and efficient mechanical actuators (such as PZTs) dedicated to repetition-rate tuning. For the silica microcomb characterized in this work, jitter characterization without disturbing the comb operation is particularly desirable because a continuous feedback control to the pump is required for maintaining soliton operation [see Fig. 1(a)].

Figure 2 shows the schematic of timing jitter characterization. A more complete description of the method itself can be found in Ref. [38]; here, we briefly summarize its operation principle and the modifications that we have made for characterizing microcombs. Each comb line is written as $f_k = kf_{rep} + f_{ceo}$ ($k = 1, 2, 3, \ldots$), where f_{rep} is the repetition rate and f_{ceo} is the carrier-envelope-offset frequency. Two frequency modes (f_n and f_m) are used to extract the phase noise in repetition rate only (i.e., $(m - n)f_{rep}$) by subtracting the common-mode f_{ceo} noise in the comb line. In the experiment, 1540 nm ($f_m = 194.81$ THz) and 1560 nm ($f_n = 192.31$ THz) with 2-nm FWHM bandwidth are filtered by fiber Bragg gratings. A Mach–Zehnder interferometer with a long fiber delay line (60-m long, equivalent to time delay of $\tau = 300$ ns) in one arm is used for enhancing the timing detection sensitivity, which is proportional to the delay time. The delay line is implemented by using a 60-m-long fiber PZT stretcher. Since two frequency modes have different group velocities in the fiber, a delay control unit (DCU) is implemented in the fiber delay line for concurrent interference at the interferometer output [38]. An acousto-optic frequency shifter (AOFS) is also inserted in the fiber delay line to avoid unwanted background noise in the baseband by synchronous detection. The interferometer output then contains the frequency noise of each frequency mode weighted by the delay time (τ) in the form of the phase noise at f_{aom}, as $\delta[\tau(nf_{rep} + f_{ceo} + f_{aom})]$ and $\delta[\tau(mf_{rep} + f_{ceo} + f_{aom})]$. Note that both f_m and f_n components traveling through the delay line are modulated by f_{aom} and that is why it can appear in both terms. While longer delay time ensures better sensitivity, there is a trade-off with the measurement bandwidth (that scales with $1/\tau$). In this work, a 60-m long delay is selected to ensure both high sensitivity (20 zs/Hz$^{1/2}$) and broad jitter analysis bandwidth (3.3 MHz). The photodetected signal of each mode is filtered at f_{aom} and mixed by an RF mixer to reject the common-mode f_{ceo} noise. This downconverted RF mixer output contains the repetition-rate phase noise or timing jitter as a form of $\delta[\tau(m - n)f_{rep}]$.

The final step is to analyze the baseband noise, and the delay should be locked to the comb under test to prevent the frequency
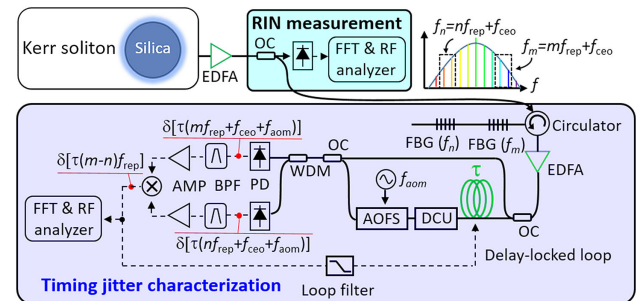

Fig. 1. Schematic of the soliton generation and characteristics of the silica resonator. (a) Schematic of the soliton generation from a silica-based microcomb. EDFA, erbium-doped fiber amplifier; AOM, acousto-optic modulator; NF, notch filter; OC, optical coupler; (b) measured dispersion of the mode for soliton generation; ω_μ, resonant frequency in radians per second with respect to micrometer, the relative mode number with respect to pump; ω_0, pump frequency in radians per second; D_1, free spectral range (FSR) in radians per second; (c) measured optical spectrum and squared hyperbolic secant envelope (red solid curve); (d) measured intensity autocorrelation (black dots) and its sech^2 fitting (red curve); (e) RF spectra of the generated soliton pulse train; RBW, resolution bandwidth.

Fig. 2. Schematic of timing jitter characterization using a fiber delay line and RIN measurement. RIN, relative intensity noise; OC, optical coupler; FBG, fiber Bragg grating; EDFA, erbium-doped fiber amplifier; AOFS, acousto-optic frequency shifter; DCU, delay control unit; WDM, wavelength division multiplexing coupler; AMP, RF amplifier; BPF, bandpass filter; PD, photodetector.

drift during the measurement. For this, we apply $\delta[\tau(m-n)f_{rep}]$ signal to the PZT stretcher in the fiber delay line, forming a delay-locked loop (DLL). It is important to keep the locking bandwidth as low as possible to ensure broadband characterization because the free-running comb jitter can be analyzed only outside the DLL locking bandwidth. In this work, we used a 300 Hz locking bandwidth. As a result, the jitter PSD from 300 Hz to 3.3 MHz could be measured. The measured voltage PSD is converted to the frequency noise by the transfer function $T(f)$

$$T(f) = V_{pk}\frac{|1 - e^{-i2\pi f\tau}|}{|i \times f|}(V/Hz),\qquad(1)$$

where V_{pk} is half of the peak-to-peak voltage from the mixer output and τ is the delay time. This frequency noise is converted to the equivalent timing jitter or repetition-rate phase noise.

In addition to the jitter measurement, the relative intensity noise (RIN) is also characterized. To measure RIN, 1 mW optical power is tapped off. The RIN measurement is not limited by thermal noise (-173 dB/Hz) and shot noise ((-157 dB/Hz)) of the photodetector, which are much lower than the measured RIN levels [Fig. 3(a)].

Curve (i) of Fig. 3(b) shows the measured timing jitter PSD result both in s^2/Hz and dBc/Hz (at 22-GHz carrier) units. The measurement background noise is 20 zs/Hz$^{1/2}$ ($4 \times$
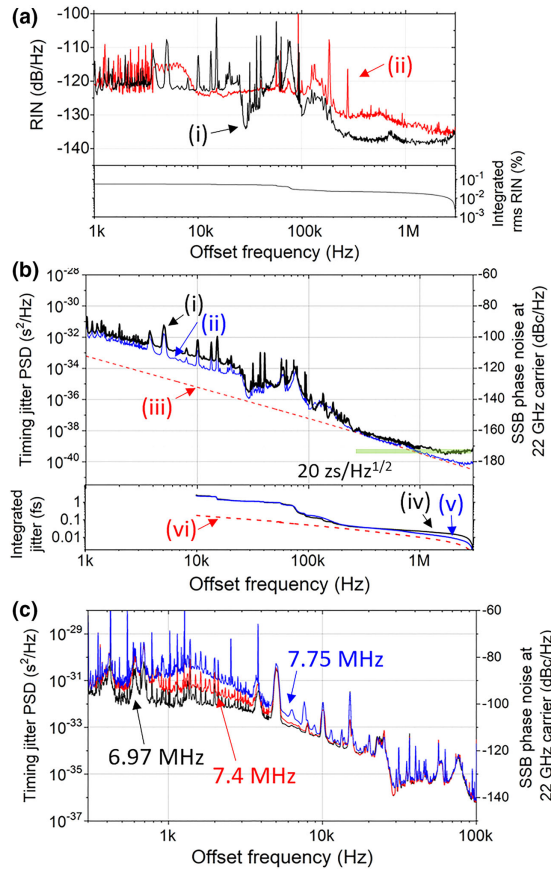
Fig. 3. Measured RIN and timing jitter (i.e., f_{rep} phase noise). (a) Measured RIN of the soliton [curve (i)] and the pump [curve (ii)]; (b) measured timing jitter [curve (i)], projected timing jitter from soliton RIN [curve (ii)], and computed quantum limit of timing jitter using comb parameters [curve (iii)]. Integrated rms timing jitter of curves (i)–(iii) are curves (iv)–(vi), respectively; (c) measured timing jitter PSDs depending on the cavity detuning.

10^{-40} s^2/Hz), which limits the jitter measurement for >1.5 MHz offset frequency range. The measured timing jitter PSDs at 10 kHz, 100 kHz, and 1 MHz offset frequencies are 6.8×10^{-34} s^2/Hz, 3.6×10^{-37} s^2/Hz, 7.3×10^{-40} s^2/Hz, respectively. The rms timing jitter is 2.6 fs when integrated from 10 kHz to 3 MHz offset frequency, where >10 kHz offset frequency is the typically used integration range for quoting timing jitter for telecommunication and signal processing applications [42]. Note that this jitter performance was obtained by finding the optimal operation condition (quiet point [24,32]) by changing the cavity detuning. As shown in Fig. 3(c), finding the right cavity detuning could effectively reduce the timing jitter below 10 kHz offset frequency.

One of the well-known limiting factors for timing jitter in microcombs is the intensity noise-coupled jitter, since the soliton generation via four-wave mixing is highly affected by the intensity noise. The intensity noise-coupled phase noise (timing jitter) scales as a form of $L_\phi(f) = C \times S_I(f)/f^2$, where C is the fitting coefficient and $S_I(f)$ is the RIN. The pump RIN can be coupled to the timing jitter via cavity detuning [23]. On the other hand, soliton RIN can be also coupled to the timing jitter via intracavity nonlinearity such as the self-steepening effect [43–45]. In this work, by accurately measuring both pump RIN and soliton output RIN spectra [Fig. 3(a)] and comparing the projected RIN-originated jitter PSDs with the measured jitter PSD (see Fig. S2 of Supplement 1), we could observe that the projected soliton RIN-coupled jitter [curve (ii) in Fig. 3(b)] fits fairly well with the measured jitter [curve (i) in Fig. 3(b)] for the 1 kHz–1 MHz offset frequency range (within ~3 dB for most of the range, with the maximum deviation of ~6 dB in the 10 kHz–20 kHz range). Note that we also experimentally confirmed that the amplitude-to-timing conversion in the jitter measurement setup is extremely low, and the soliton RIN itself does not influence the accuracy of jitter measurement (see Fig. S3 of Supplement 1). Further theoretical and experimental study on this soliton RIN-coupled jitter will be necessary as a future work.

We also compared the measured jitter with the computed quantum limit in single sideband (SSB) phase noise PSD [28,36]:

$$L_\phi(f) = \frac{\sqrt{2}\pi}{2}\sqrt{\frac{\gamma}{\Delta_0(-D)}}\frac{g}{\eta\gamma^2}$$
$$\times\left[\frac{1}{96}\frac{\gamma(-D)}{\Delta_0}\frac{\eta\gamma^2}{f^2} + \frac{1}{24}\left(1 + \frac{\pi^2 f^2}{\gamma^2}\right)^{-1}\frac{\eta\gamma^2}{\pi^2 f^2}\frac{\Delta_0(-D)}{\gamma}\right],$$
$$(2)$$

where $2\gamma (= 1.2 \times 10^7$ rad/s) is the FWHM resonance linewidth, $\Delta_0 (= 4.4 \times 10^7$ rad/s) is the measured optical detuning [36,46], $g (= 1.6 \times 10^{-3}$ rad/s) is the frequency shift of a resonant mode per photon [36], $D (= -0.017)$ is the normalized group velocity dispersion [36], and $\eta (= 1)$ is the quantum efficiency of the detector. Note that the shot-noise term is removed from Eq. 68 of Ref. [36] because our measurement is not limited by the shot noise of photodetection. The measurement result [curve (i)] closely approaches the theoretical prediction of the quantum limit [curve (iii)] in the 300 kHz–1 MHz range.

In summary, we have shown 2.6-fs rms timing jitter [10 kHz–3 MHz] of the 22-GHz silica microcomb, which shows the true timing performance of microcombs not limited by the measurement resolution. In particular, on-chip silica microcombs can achieve ultralow timing jitter from an integrated photonic

platform, which shows its high potential for on-chip microwave photonic applications. The demonstrated jitter performance can already overcome today's jitter limitations in high-speed signal processing: for example, 2.6-fs aperture jitter at 22-GHz corresponds to 12 effective-number-of-bit (ENOB) resolution for analog-to-digital conversion of 11-GHz bandwidth signal, where the current state of the art is 7 ENOB [47]. Our measurement result suggests that suppressing intensity noise will be an effective way to further reduce timing jitter of microcombs. As anticipated from the results shown in Fig. 3(b), by fully suppressing intensity noise-coupled jitter, a free-running silica microcomb may potentially achieve 200-as-level timing jitter over a 0.1-ms time scale.

Disclosures. The authors declare no conflicts of interest.

Please see Supplement 1 for supporting content.

[†]These authors contributed equally to this work.

REFERENCES

1. T. J. Kippenberg, R. Holzwarth, and S. A. Diddams, Science **332**, 555 (2011).
2. P. Del'Haye, A. Schliesser, O. Arcizet, T. Wilken, R. Holzwarth, and T. Kippenberg, Nature **450**, 1214 (2007).
3. J. S. Levy, A. Gondarenko, M. A. Foster, A. C. Turner-Foster, A. L. Gaeta, and M. Lipson, Nat. Photonics **4**, 37 (2010).
4. A. A. Savchenkov, A. B. Matsko, V. S. Ilchenko, I. Solomatine, D. Seidel, and L. Maleki, Phys. Rev. Lett. **101**, 093902 (2008).
5. D. Braje, L. Hollberg, and S. Diddams, Phys. Rev. Lett. **102**, 193902 (2009).
6. D. T. Spencer, T. Drake, T. C. Briles, J. Stone, L. C. Sinclair, C. Fredrick, Q. Li, D. Westly, B. R. Ilic, A. Bluestone, N. Volet, T. Komljenovic, L. Chang, S. H. Lee, D. Y. Oh, M.-G. Suh, K. Y. Yang, M. H. P. Pfeiffer, T. J. Kippenberg, E. Norberg, L. Theogarajan, K. Vahala, N. R. Newbury, K. Srinivasan, J. E. Bowers, S. A. Diddams, and S. B. Papp, Nature **557**, 81 (2018).
7. M.-G. Suh, Q. Yang, K. Yang, X. Yi, and K. J. Vahala, Science **354**, 600 (2016).
8. P. Trocha, M. Karpov, D. Ganin, M. H. P. Pfeiffer, A. Kordts, S. Wolf, J. Krockenberger, P. Marin-Palomo, C. Weimann, S. Randel, W. Freude, T. J. Kippenberg, and C. Koos, Science **359**, 887 (2018).
9. E. Obrzud, M. Rainer, A. Harutyunyan, M. H. Anderson, M. Geiselmann, B. Chazelas, S. Kundermann, S. Lecomte, M. Cecconi, A. Ghedina, E. Molinari, F. Pepe, F. Wildi, F. Bouchy, T. J. Kippenberg, and T. Herr, Nat. Photonics **13**, 31 (2019).
10. T. M. Fortier, M. S. Kirchner, F. Quinlan, J. Taylor, J. C. Bergquist, T. Rosenband, N. Lemke, A. Ludlow, Y. Jiang, C. W. Oates, and S. A. Diddams, Nat. Photonics **5**, 425 (2011).
11. X. Xie, R. Bouchand, D. Nicolodi, M. Giunta, W. Hänsel, M. Lezius, A. Joshi, S. Datta, C. Alexandre, M. Lours, P.-A. Tremblin, G. Santarelli, R. Holzwarth, and Y. L. Coq, Nat. Photonics **11**, 44 (2017).
12. J. Kim, J. A. Cox, J. Chen, and F. X. Kärtner, Nat. Photonics **2**, 733 (2008).
13. S. Schulz, I. Grguraš, C. Behrens, H. Bromberger, J. T. Costello, M. K. Czwalinna, M. Felber, M. C. Hoffmann, M. Ilchen, H. Y. Liu, T. Mazza, M. Meyer, S. Pfeiffer, P. Prędki, S. Schefer, C. Schmidt, U. Wegner, H. Schlarb, and A. L. Cavlieri, Nat. Commun. **6**, 5938 (2015).
14. I. Coddington, W. C. Swann, L. Nenadovic, and N. R. Newbury, Nat. Photonics **3**, 351 (2009).
15. Y. Na, C. Jeon, C. Ahn, M. Hyun, D. Kwon, J. Shin, and J. Kim, Nat. Photonics **14**, 355 (2020).
16. G. C. Valley, Opt. Express **15**, 1955 (2007).
17. A. Khilo, S. J. Spector, M. E. Grein, A. H. Nejadmalayeri, C. W. Holzwarth, M. Y. Sander, M. S. Dahlem, M. Y. Peng, M. W. Geis, N. A. DiLello, J. U. Yoon, A. Motamedi, J. S. Orcutt, J. P. Wang, C. M. Sorace-Agaskar, M. A. Popovic, J. Sun, G. R. Zhou, H. Byun, J. Chen, J. L. Hoyt, H. I. Smith, R. J. Ram, M. Perrott, T. M. Lyszczarz, E. P. Ippen, and F. X. Kärtner, Opt. Express **20**, 4454 (2012).
18. J. Pfeifle, V. Brasch, M. Lauermann, Y. Yu, D. Wegner, T. Herr, K. Hartinger, P. Schindler, J. Li, D. Hillerkuss, R. Schmogrow, C. Weimann, R. Holzwarth, W. Freude, J. Leuthold, T. Kippenberg, and C. Koos, Nat. Photonics **8**, 375 (2014).
19. C. Debaes, A. Bhatnagar, D. Agarwal, R. Chen, G. A. Keeler, N. C. Helman, H. Thienpont, and D. A. B. Miller, IEEE J. Sel. Top. Quantum Electron. **9**, 400 (2003).
20. A. J. Benedick, J. G. Fujimoto, and F. X. Kärtner, Nat. Photonics **6**, 97 (2012).
21. T. K. Kim, Y. Song, K. Jung, C. Kim, H. Kim, C. H. Nam, and J. Kim, Opt. Lett. **36**, 4443 (2011).
22. J. Kim and Y. Song, Adv. Opt. Photon. **8**, 465 (2016).
23. J. R. Stone, T. C. Briles, T. E. Drake, D. T. Spencer, D. R. Carlson, S. A. Diddams, and S. B. Papp, Phys. Rev. Lett. **121**, 063902 (2018).
24. X. Yi, Q.-F. Yang, X. Zhang, K. Y. Yang, and K. Vahala, Nat. Commun. **8**, 14869 (2017).
25. X. Yi, Q.-F. Yang, K. Y. Yang, M.-G. Suh, and K. Vahala, Optica **2**, 1078 (2015).
26. E. S. Lamb, D. R. Carlson, D. D. Hickstein, J. R. Stone, S. A. Diddams, and S. B. Papp, Phys. Rev. Appl. **9**, 024030 (2018).
27. N. Kuse, T. C. Briles, S. Papp, and M. Fermann, Opt. Express **27**, 3873 (2019).
28. S.-W. Huang, J. Yang, M. Yu, B. H. McGuyer, D. L. Kwong, T. Zelevinsky, and C. W. Wong, Sci. Adv. **2**, e1501489 (2016).
29. J. Liu, E. Lucas, A. S. Raja, J. He, J. Riemensberger, R. N. Wang, M. Karpov, H. Guo, R. Bouchand, and T. J. Kippenberg, Nat. Photonics **14**, 486 (2020).
30. W. Liang, D. Eliyahu, V. S. Ilchenko, A. A. Savchenkov, A. B. Matsko, D. Seidel, and L. Maleki, Nat. Commun. **6**, 7957 (2015).
31. W. Weng, E. Lucas, G. Lihachev, V. E. Lobanov, H. Guo, M. L. Gorodetsky, and T. J. Kippenberg, Phys. Rev. Lett. **122**, 013902 (2019).
32. Z. Pi and F. Khan, IEEE Commun. Mag. **49**(6), 101 (2011).
33. H. Lee, T. Chen, J. Li, K. Y. Yang, S. Jeon, O. Painter, and K. J. Vahala, Nat. Photonics **6**, 369 (2012).
34. K. Y. Yang, D. Y. Oh, S. H. Lee, Q.-F. Yang, X. Yi, B. Shen, H. Wang, and K. Vahala, Nat. Photonics **12**, 297 (2018).
35. M. Suh and K. Vahala, Optica **5**, 65 (2018).
36. A. B. Matsko and L. Maleki, Opt. Express **21**, 28862 (2013).
37. K. Jung and J. Kim, Sci. Rep. **5**, 16250 (2015).
38. D. Kwon, C. G. Jeon, J. Shin, M. S. Heo, S. E. Park, Y. Song, and J. Kim, Sci. Rep. **7**, 40917 (2017).
39. T. Herr, V. Brasch, J. D. Jost, I. Mirgorodskiy, G. Lihachev, M. L. Gorodetsky, and T. J. Kippenberg, Phys. Rev. Lett. **113**, 123901 (2014).
40. X. Yi, Q.-F. Yang, K. Youl Yang, and K. Vahala, Opt. Lett. **41**, 2037 (2016).
41. T. Herr, V. Brasch, J. D. Jost, C. Y. Wang, N. M. Kondratiev, M. L. Gorodetsky, and T. J. Kippenberg, Nat. Photonics **8**, 145 (2014).
42. Keysight Technologies. "E8257D PSG microwave analog signal generator:data sheet," 2017, https://www.keysight.com/us/en/assets/7018-01211/data-sheets/5989-0698.pdf.
43. R. Paschotta, Appl. Phys. B **79**, 163 (2004).
44. E. Lucas, P. Brochard, R. Bouchand, S. Schilt, T. Sudmeyer, and T. J. Kippenberg, Nat. Commun. **11**, 374 (2020).
45. Y. Wang, H. Tian, D. Hou, F. Meng, Y. Ma, H. Xu, F. X. Kärtner, Y. Song, and Z. Zhang, Opt. Express **27**, 11273 (2019).
46. E. Lucas, H. Guo, J. D. Jost, M. Karpov, and T. J. Kippenberg, Phys. Rev. A **95**, 043822 (2017).
47. S. Gupta and B. Jalali, Opt. Lett. **33**, 2674 (2008).